Contact cluster modeling of allosteric communication in PDZ domains

Emanuel Dorbath, Fabian Rudolf, Adnan Gulzar, and Gerhard Stock*

Biomolecular Dynamics, Institute of Physics, University of Freiburg, 79104 Freiburg, Germany

E-mail: stock@physik.uni-freiburg.de

Abstract

Allostery, the intriguing phenomenon of longrange communication between distant sites in proteins, plays a central role in biomolecular regulation and signal transduction. While it is commonly attributed to conformational rearrangements, the underlying dynamical mechanisms remain poorly understood. The contact cluster model of allostery [J. Chem. Theory Comput. 2024, 20, 10731 identifies localized groups of highly correlated contacts that mediate interactions between secondary structure elements. This framework proposes that allostery proceeds through a multistep process involving cooperative contact changes within clusters and communication between distant clusters, transmitted through rigid secondary structures. To demonstrate the validity and generality of the model, this Perspective employs extensive molecular dynamics simulations ($\sim 1 \,\mathrm{ms}$ total simulation time) of four different photoswitchable PDZ domains and studies how different domains, ligands and perturbations influence both the contact clusters and their dynamical evolution. These analyses reveal several recurring clusters that represent shared flexible structural modules, such as loops connecting β -sheets, and show that the characteristic timescales of the nonequilibrium protein response can be directly associated with the motions of individual contact clusters. Thus, the dynamic decomposition of PDZ domains into contact clusters uncovers a modular, dynamics-based architecture that underlies and facilitates long-range allosteric communication.

Introduction

Allostery is a fundamental mechanism by which proteins regulate essential cellular processes, such as signal transduction and enzymatic activity, by enabling long-range communication between distant protein sites. A comprehensive understanding of allostery requires not just a static picture of protein structure, but insight into both the protein's structure and its conformational dynamics mediating functional coupling.^{2–9} However, the direct observation of allosteric transitions remains difficult, particularly because of the subtle nature of structural changes 10-12 and due to the limited sampling of molecular dynamics (MD) simulations. 13-17 Hence, allosteric communication is most commonly explained through network models, ^{18,19} which describe protein residues as the nodes of the network, while the edges represent interresidue couplings. Although these models have significantly advanced our understanding of allostery, they do not provide the real-time evolution of the allosteric transition, which is the ultimate goal here.

PDZ domains have become a minimal model for investigating allosteric communication, because of their well-characterized allosteric properties and compact size. $^{20-27}$ They share a conserved secondary structure of two or three α -helices and six β -strands. A prominent example

is the third PDZ domain (PDZ3, Fig. 1a), which exhibits coupling between its ligand-binding pocket and the α_3 -helix at the C-terminal end. This was shown in an NMR study by Petit et al., ²¹ where removing the α_3 -helix caused a 21-fold reduction in ligand-binding affinity, providing strong evidence for intradomain allosteric communication. To achieve a timeresolved view of this process, Hamm and coworkers²⁸ incorporated a photoswitch into the α_3 -helix, triggering a conformational change in PDZ3 that propagated through the protein and caused a distant response within 200 ns. The group further performed time-resolved infrared experiments on other photoswitchable PDZ domains, revealing complex dynamics encompassing multiple timescales over seven orders of magnitude. ^{28–30} However, linking these timescales to specific molecular processes has remained challenging.

The experiments described above were paired with extensive nonequilibrium MD simulations, 15,30,31 which, in principle, offer a fully microscopic view of the allosteric transition. The challenge, however, lies in distilling the vast amount of simulation data into a simple, low-dimensional model that still captures the underlying mechanism. 32,33 To address this, Buchenberg et al. 15 applied principal component analysis to backbone dihedral angles³⁴ for a PDZ2 domain with a cross-linked photoswitch. Alternatively, Bozovic et al. 30 constructed a Markov state model^{35,36} from selected C_{α} -distances, obtained from MD data of a PDZ2 domain bound to a photoswitched ligand. While these models reproduced the experimental timescales, they did not fully resolve the underlying mechanism.

The success of dimensionality reduction and molecular mechanism modeling hinges on selecting initial coordinates (or features) that capture the essential processes. ^{34,37,38} This involves two steps: the definition of suitable features and some selection process to discard irrelevant noise. Firstly, guided by comprehensive prior studies, ^{38–43} we use interresidue contact distances—encompassing hydrogen bonds, salt bridges, and nonpolar contacts—as our features. We assume that a con-

tact is formed if the distance between the closest non-hydrogen atoms of two non-neighboring residues is shorter than 4.5 Å, see Methods. Because contact distances emphasize short-range interactions, they directly reflect the microscopic mechanism while also capturing longrange structural changes that arise as downstream consequences. (Analogously, in a mechanical machine, the contacts would be the cogwheels of the gearing, and the long-range changes the lever arms performing a function.) Secondly, in most proteins, only a small subset of these coordinates is involved in a given biomolecular process, making it crucial to discard uncorrelated noise or weakly correlated motions. To achieve this, we apply the Leiden community detection-based feature selection method MoSAIC, 44 which identifies correlated dynamics and partitions proteins into modular subunits—referred to as clusters—based on dynamic connectivity.

To illustrate the explanatory power of these contact clusters, we briefly revisit the above mentioned experimental study²⁸ on photoswitchable PDZ3, which revealed a nonequilibrium response on timescales from subnanoseconds to tens of microseconds. interpret these results, Ali et al. 31,45 performed extensive nonequilibrium MD simulations of PDZ3, determined the contact distances $r_i = r(a, b)$ between residues a and b, and monitored their time evolution. As representative examples, Fig. 1b shows the ensemble average of distances r(101, -4) (between the the initially excited α_3 -helix and the ligand) and r(24,0) (between the distant β_2 -sheet and the ligand). To characterize the timescales of their evolution, they performed a timescale analysis 46

$$r_j(t) = \sum_k a_{kj} e^{-t/\tau_k}, \qquad (1)$$

where the time constants τ_k are equally distributed on a logarithmic scale (e.g., 10 terms per order of magnitude) and the corresponding amplitudes a_{kj} are fitted to the data, using a maximum-entropy regularization method, ⁴⁷ see Methods.

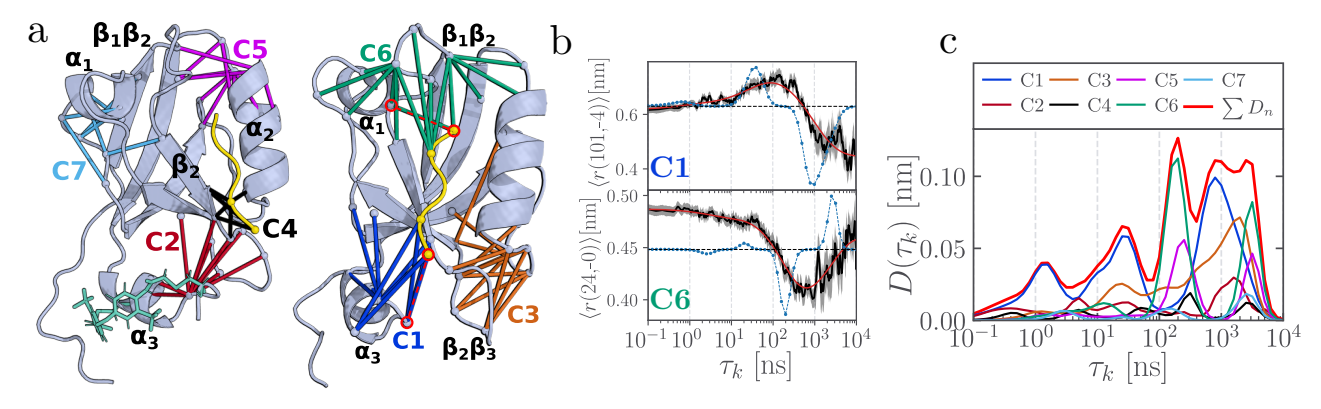


Figure 1: Structure and nonequilibrium response of a photoswitchable PDZ3 domain. ²⁸ (a) Illustration including main secondary structural elements, the azobenzene photoswitch (green; shown only on the left), and the ligand (KETWV, yellow) located in the binding pocket between the β_2 -strand and the α_2 -helix. Colored lines indicate the contact distances associated with clusters C1–C7, as identified by MoSAIC. ⁴⁴ (b) Time evolution of contact distances r(101, -4) located in cluster C1 and r(24, 0) located in cluster C6, see circled distances in panel (a). (Residues are numbered from 1 to 103 for the protein and from -4 to 0 for the ligand.) MD data are drawn in black, their confidence interval (standard error of the mean) is indicated as gray area, the timescale spectrum $[a_{kj}(\tau_k)]$ in Eq. (1) in blue, and the resulting fit of the data [Eq. (1)] in red. The increase of the fluctuations in the last decade is due to the reduced number of trajectories for $t \ge 1\mu$ s, cf. Tab. 1. (c) Dynamical content [Eq. (2)] derived from timescale analyses of the contact distances for all clusters combined (bold red) and each individual cluster.

Indicated by blue lines in Fig. 1b, the analysis reveals that distance r(101, -4) increases and decreases on timescales of 30 and 800 ns, respectively, while r(24,0) responds not before 200 ns and then again at $3 \mu s$. The overall response of the system can be quantified via the dynamical content ⁴⁶

$$D(\tau_k) = \sqrt{\sum_j |a_{kj}|^2}, \qquad (2)$$

which sums up the response of all considered features. As shown in Fig. 1c, $D(\tau_k)$ reveals peaks at times 1, 30, 200, 800, and 3000 ns, which are found to closely match the experimental results.²⁸

To explain these timescales in terms of molecular motion, Ali et al. 45 carried out a MoSAIC analysis 44 on PDZ3 (see Fig. S1 and Methods) which block-diagonalizes the contact distance correlation matrix, thus identifying seven localized contact clusters shown in Fig. 1a. Calculation of the dynamical content D_n for each cluster n (Fig. 1c) allowed the assignment of individual peaks to distinct processes: photoswitching of the α_3 -helix at t=0 initiates its gradual

detachment, producing two peaks in cluster C1 at 1 and 30 ns. This is followed by activation of the distant cluster C6 at 200 ns, which in turn induces a back-reaction in C1 at 800 ns, accounting for the re-alignment of the α_3 -helix. Finally, at $\sim 3\mu$ s, structural relaxation occurs in clusters C5, C6 and C7. The contact-cluster framework thus reveals the long-range communication between the initially perturbed cluster C1 and the distant cluster C6, providing a direct mechanistic picture of the allosteric transition in PDZ3.

While the example of PDZ3 provides a clear validation of this strategy, it is important to assess its generality—both in terms of (i) the identification of contact clusters and (ii) their dynamical evolution. If contact clusters are intrinsic features of a protein, we would expect:

- Contact clusters to be identifiable from standard equilibrium MD simulations.
- Similar proteins, such as different PDZ domains, to exhibit similar contact clusters.
- Nonequilibrium studies initiated with different perturbations to be explainable us-

Table 1: Considered PDZ domains and equilibrium (EQ) and nonequilibrium (NEQ) simulations.

system	ligand	MD runs
PDZ3WT ³¹	KETWV	EQ: $4 \times 1 \mu s$
$PDZ3^{31,45}$	KETWV	NEQ: $90 \times 1 \mu s$;
PDZ3L6	KKETWV	NEQ: $89 \times 1 \mu s$ $10 \times 10 \mu s$
$PDZ2S^{15}$	_	NEQ: $14 \times 10 \mu s$
PDZ2L ³⁰	RWAKSEAK	NEQ: $80 \times 1 \mu s$;
	ECEQVSCV	$19 \times 10 \mu s$

ing the same set of contact clusters.

To address these questions, we revisit nonequilibrium studies of various PDZ domains, determine their contact clusters, and examine how different ligands and perturbations influence both the clusters and their dynamical evolution. Specifically, we analyze: a PDZ3 domain bound to a longer ligand (PDZ3L6), a PDZ2 domain with a photoswitch cross-linked over the binding pocket 15,29 (PDZ2S), and a PDZ2 domain with a photoswitchable ligand³⁰ (PDZ2L). Table 1 summarizes all systems and simulations, while the Supplementary Information (SI) provides each protein's sequence and secondary structure, the MoSAIC correlation matrix, the list of contacts included in the clusters, and their nonequilibrium time evolution. We begin by identifying the contact clusters of wild-type PDZ3 (PDZ3WT) from equilibrium MD simulations and comparing them with those obtained from nonequilibrium studies. For this system, we also examine the advantages and limitations of using either nearest heavy-atom contact distances or the corresponding C_{α} -distances as features for defining functionally relevant clusters.

Results and discussion

Calculating contact clusters from equilibrium simulations

The contact clusters shown in Fig.1a were derived from nonequilibrium (NEQ) simulations of photoswitchable PDZ3, in which the azobenzene photoswitch was initially switched from

a twisted cis to a stretched trans configuration. 31 In addition to these simulations, Ali et al. 31 performed standard MD simulations of the cis and trans equilibrium (EQ) states, as well as of the wild-type protein without the photoswitch. Here, we applied MoSAIC clustering to the contact distances of all these trajectories (see Fig. S4). As an example, Fig. 2a shows the contact clusters identified for PDZ3WT (EQ), which can be directly compared to the clusters of PDZ3 (NEQ) in Fig. 1a. In both cases, seven clusters are found, localized in the same regions of the protein. The lists of contact distances are not identical (see Tabs. S2 and S4). as expected given that the two systems differ in the presence or absence of the azobenzene photoswitch on the α_3 -helix. Consistently, when comparing contact distances from NEQ and EQ simulations of the same photoswitchable PDZ3 (Tab. S3), the agreement is even stronger.

We therefore conclude that contact clusters are indeed intrinsic features of a protein, comprising functionally relevant contacts that mediate tertiary interactions between relatively rigid secondary-structure elements. Acting as flexible joints or hinges, these regions play a critical role in enabling structural rearrangements. ⁴⁸

Feature Selection: Contact vs. C_{α} distances

Several definitions of inter-residue distance can be employed. In our approach, contacts are identified based on the shortest heavy-atom distance between two non-neighboring residues being below 0.45 nm. 41,43 This criterion is computationally demanding, as it requires monitoring all heavy-atom distances for every residue pair throughout an MD trajectory. Using the Python package msmhelper 49 on a standard desktop computer with 10 physical cores, this calculation typically takes about 2 hours for a protein of 10^2 residues and roughly 9 hours for a protein of 10^3 residues, each analyzed over 10^6 MD frames.

Requiring about an order of magnitude less computation time, we can alternatively monitor the distance between the corresponding C_{α} -

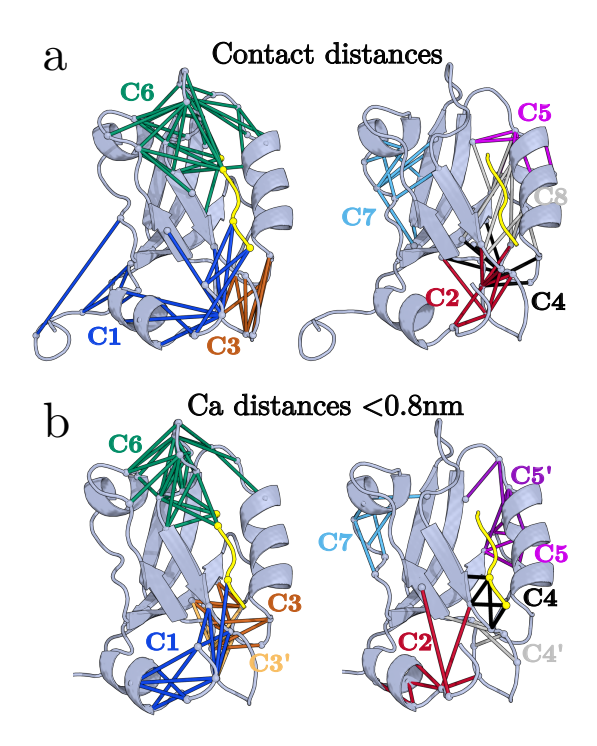


Figure 2: Contact clusters C1 to C7 of PDZ3WT obtained from equilibrium MD simulations. Compared are contact clusters obtained from (a) shortest heavy-atom interresidue distances below 0.45 nm and (b) corresponding C_{α} -distances below 0.8 nm.

atoms, and require this distance to remain below 0.8 nm for at least 10% of the simulation time, see Tab. S5. To compare these "local" C_{α} -distances with the nearest heavy-atom contact distances, Fig. 2b shows the resulting contact clusters for PDZ3WT. In both cases, we obtain seven clusters localized in the same regions of the protein, indicating that local C_{α} distances provide, on average, a good approximation to the heavy-atom contact distances. Nonetheless, for elucidating the mechanism of a structural change, contact distances are generally preferable, as the formation or breaking of a contact often coincides with local structural stabilization or destabilization. In addition, changes in backbone hydrogen bonds directly affect the amide I band (primarily backbone C=O stretch vibrations), which can facilitate comparisons between MD simulations and infrared spectroscopy data. 12

Finally, we briefly highlight two alternative approaches for using inter-residue distances as features. First, several studies⁵⁰ have discussed

the benefits of employing inverse distances, particularly because they offer greater sensitivity at shorter distances. When assessing the dynamical content for this approach, Fig. S3 shows that, for PDZ3, the change in dynamical content is minimal. On the other hand, we note that in Markov state modeling it is common to use all N(N-1)/2 C_{α}-distances as features. ^{37,51} For PDZ3WT, we examined this choice in the SI and showed that the resulting main MoSAIC clusters primarily contain distances than span from one or a few anchor points all across over the entire protein (Fig. S6). These clusters mostly capture global protein motions, similar to those observed in normal mode analysis (Fig. S7). However, while normal mode analysis mainly captures non-reactive ground-state fluctuations, our focus is on describing the reaction mechanism driven by contact changes. For this purpose, local C_{α} -distances (i.e., $d \leq 0.8 \,\mathrm{nm}$, see Fig. 2b) may be useful, while including all C_{α} -distances tends to be counter-productive.

PDZ3L6: Modifying the ligand

We now study how contact clusters and nonequilibrium response of the photoswitchable PDZ3 domain shown in Fig. 1 are affected by a small modification of the system. As a test case, we consider the same PDZ3 domain, but with a ligand (KKETWV) that is extended by one additional Lys residue. Performing a Mo-SAIC correlation analysis on the MD data of this variant (hereafter referred to as PDZ3L6), we again obtain seven contact clusters. Figure 3a reveals that these clusters closely resemble those identified for PDZ3 in Fig. 1a (cf. Tabs. S2) and S6). The only notable (and expected) difference is cluster C1, which exclusively involves contacts with the extra ligand residue Lys(-5): three to the α_3 -helix, two to the protein core, and one to the ligand residue Thr(-2). Recall that in PDZ3, cluster C1 contains 11 contacts, with several between the α_3 -helix and various ligand residues (see Tab. S2). Hence, the addition of a single residue, Lys(-5), completely reshapes the contact network of C1, while leaving the other clusters largely unaffected.

Since cluster C1 is the primary site excited by

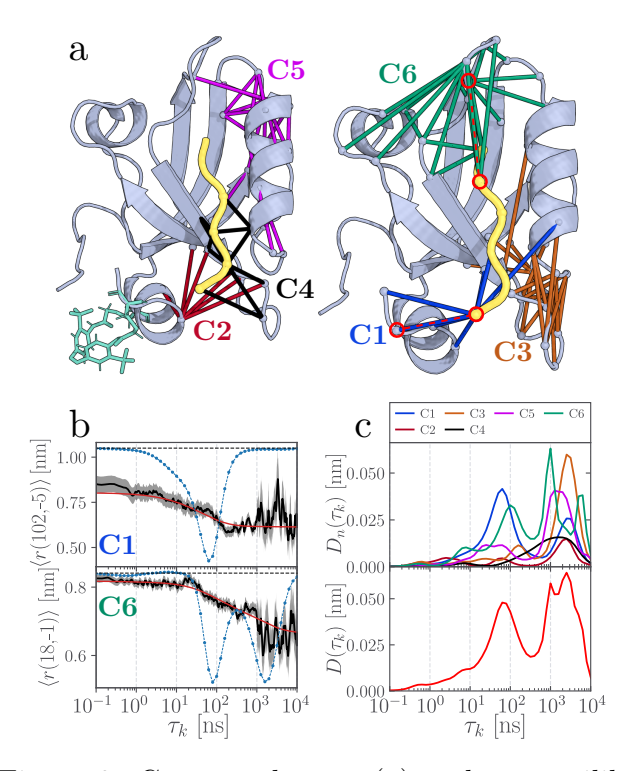


Figure 3: Contact clusters (a) and nonequilibrium response (b,c) of a photoswitchable PDZ3 domain (PDZ3L6) with a ligand that is one residue longer than the PDZ3 shown in Fig.1. See the caption of Fig.1 for additional information.

photoswitching of the α_3 -helix, it is instructive to examine how the nonequilibrium response of PDZ3L6 differs from that of PDZ3. As an example, Fig. 3b depicts the time evolution of the contact distance r(102, -5), which exhibits a single decay on a timescale of $\sim 80\,\mathrm{ns}$. Accordingly, the dynamical content of PDZ3L6 (Fig. 3c) exhibits a first main peak at 80 ns originating from C1, followed by a weaker feature at $\sim 2 \,\mu s$ arising from C1 contacts not involving α_3 (Fig. S9). This is in contrast to the more complex dynamics of C1 in PDZ3 (Fig. 1), where the initial detachment of the α_3 -helix (at 1 and 30 ns) is succeeded by its re-alignment around 800 ns. Another notable difference of PDZ3L6 is that the response of the distant cluster C6 (distance r(18,-1)) occurs already at 100 ns (compared to 200 ns in PDZ3). This acceleration is most likely induced by the intra-ligand contact r(-5, -2), which provides a shortcut in the mechanical coupling between clusters C1 and C6. 45 At longer times, the dynamical content of PDZ3L6 reflects the combined response of clusters C1, C3, C5, and C6, which closely resembles the behavior observed for PDZ3. In summary, although the details of the short-time dynamics differ from those of PDZ3, the overall long-range coupling between C1 and the distant clusters C5 and C6 evolves in a similar manner.

PDZ2S: Cross-linking the binding pocket

Beyond the PDZ3 domains—for which recurring patterns in the contact clusters were seen—we also studied two PDZ2 variants for which the α_3 -helix is absent. In the first one, termed PDZ2S ("S" for switch), the photoswitch links residue Azo22 at the β_2 -sheet with Azo77 in the α_2 -helix. Upon cis-to-trans photoisomerization, the photoswitch therefore expands the (empty) binding pocket from an unbound-like state to a bound-like conformation, which represents a rather strong and direct perturbation. Providing a simple model of ligand binding, PDZ2S was studied by time-resolved infrared spectroscopy²⁹ and accompaning MD simulations. ¹⁵

Using the nonequilibrium simulations of Buchenberg et al., 15 we identified 330 contact distances, for which a MoSAIC analysis was carried out (Tab. S7). Figure 4a shows the resulting five contact clusters, which overall resemble those of PDZ3 (Fig. 1a), but differ in various aspects. Notably, the functionally important α_3 -helix of PDZ3 is not present in PDZ2 domains, hence clusters C1 and C2 both connected to the α_3 -helix—are not to be found in PDZ2. While both systems otherwise share the same secondary structures (2) α -helices, 6 β -strands), their sequence similarity is only 36% (Tab. S1), such that an exact correspondence of clusters is neither expected nor of particular relevance. Nevertheless, we identify similar clusters in both systems: C3 at the $\beta_2\beta_3$ -loop, C6 around the $\beta_1\beta_2$ -loop, and C7 at the α_1 -helix, although the latter contains significantly more contacts in PDZ2S. Especially the region around C6 and C7 has shown to be very important in allosteric interactions. ^{52,53} Responding directly to the photoswitching of the binding pocket, we further note the presence of a large cluster C4 at the α_2 -helix as well as a small additional cluster C8 involving the β_2 and β_3 strands.

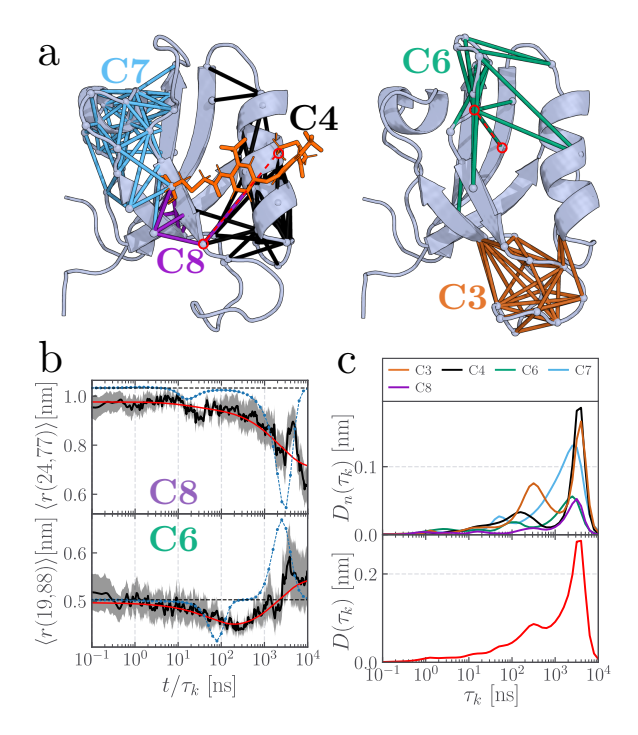


Figure 4: Contact clusters (a) and nonequilibrium response (b,c) of a PDZ2 domain (PDZ2S) featuring a photoswitch across its binding pocket. See the caption of Fig.1 for additional information.

To explore the nonequilibrium response of PDZ2S following photoswitching of its binding pocket, we again analyze the timescales of all contact distances and compute the dynamical content across all clusters (see Fig. 4b,c). The overall dynamical profile reveals two dominant peaks around 300 ns and $4 \mu s$ as well as weak features at 1 and 10 ns, which are consistent with experimental observations.²⁹ The 10 ns feature corresponds to the photoinduced opening of the binding pocket, as indicated by a first timescale in the contact distance r(24,77)within cluster C8 (Fig. 4b). The 10 ns peak appears relatively small, as only a few contacts span the binding pocket region, see Tab. S7. The same is true for the 1 ns timescale, which is caused by several contacts in clusters C4, C6 and C8 (Fig. S11), which are in direct proximity of the anchors of the photoswitch. Between 200 ns and 400 ns, we observe a broad peak that reflects the rearrangement of clusters C3 and

C4 in response to the opening of the binding pocket. The subsequent structural relaxation of these clusters gives rise to the prominent peak at $4 \mu s$, representing the fully opened binding pocket.

Interestingly, we also detect response of the two distant clusters C6 and C7, see Figs. 4b and S11. For example, distance r(19, 88) of C6 shows a transient contact change involving the $\beta_1\beta_2$ -loop, while several distances of C7 report on the ongoing destabilization of the short α_1 helix. These contacts produce small peaks at 50 and 150 ns, respectively, and contribute additional features at $2 \mu s$, thereby adding a shoulder to the dominant $4 \mu s$ peak in the overall dynamical content. Thus, despite the considerable perturbation of PDZ2S by the cross-linked photoswitch, the overall structure of the contact clusters and their dynamic response in many aspects resemble the behavior previously observed for photoswitched PDZ3. In particular, we again identify long-range coupling between the initially excited clusters (C4 and C8) and the distant clusters (C3, C6 and C7) at opposite ends of the protein.

PDZ2L: Photoswitching the ligand

The second PDZ2 variant we study contains a relatively long ligand of 16 residues, where only about half of the residues are bound to the binding pocket, see Fig. 5a. Termed PDZ2L ("L" for ligand), it differs from the other systems in that the photoswitch is attached to the ligand (at residues Azo(-1) and Azo(-6)) rather than to the protein itself.³⁰ Photoswitching azobenzene from trans-to-cis results in a squeezing of the ligand, which destabilizes its contacts in the binding pocket and ultimately leads to its unbinding. Conversely, cis-to-trans photoswitching facilitates the binding of the ligand to PDZ2L.³⁰ Compared to PDZ2S where the binding of a ligand was mimicked by the photoinduced opening of the binding pocket, the ligand-induced binding and unbinding represents a smaller and more realistic perturbation of the system.

Utilizing 441 contact distances in the Mo-

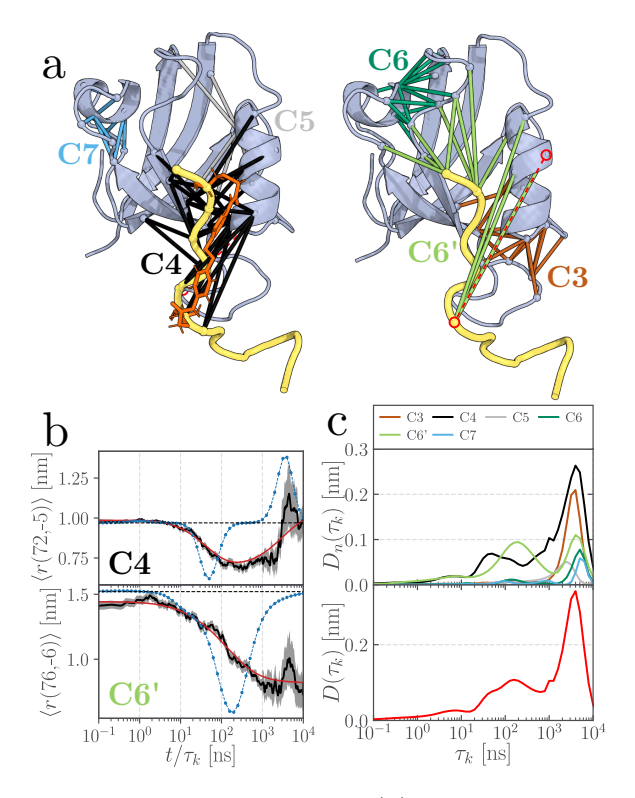


Figure 5: Contact clusters (a) and nonequilibrium response (b,c) of a PDZ2 domain (PDZ2L) featuring a photoswitched ligand across its binding pocket. See the caption of Fig.1 for additional information.

SAIC analysis, we find six functional clusters as presented in Fig. 5a. While cluster C3, C5, C6, and C7 reappear similar to the other PDZ domains, we in particular obtain clusters C4 and C6', which are located in the binding-pocket region and link ligand residues Val(0) to Glu(-7) to the PDZ2 domain. (While C6' is closely related to C6, it emerges as separate cluster in the MoSAIC analysis, see Tab. S8.) This is a direct result of the ligand unbinding being the largest and most crucial process which occurs in the system.

Monitoring the initial destabilization of the photoswitched ligand, clusters C4 and C6' exhibit an early response, yielding a broad dynamical content with peaks at 8, 30, and 150 ns of increasing amplitude (Fig. 5c). As an example monitoring this process, Fig. 5b shows the evolution of contact distances r(72, -5) of cluster C4, while distance r(76, -6) reveals the time-delayed response of cluster C6'. The dominant peak of the dynamical content at $4 \mu s$ reflects the rearrangement of virtually all contact

clusters, which indicates that the ligand has left its initial binding pose. Although hardly visible in the dynamical content, we again find several contact distances that respond already on a 1 ns timescale, see Fig. S13.

As mentioned above, Bozovic et al.³⁰ also studied the reverse reaction, i.e., the binding of the ligand to PDZ2L following cis-to-trans photoswitching. To simulate this process, the rather heterogeneous conformational distribution of the *cis* equilibrium state was sampled from the last microseconds of the trans-to-cis nonequilibrium simulations. Taking randomly chosen snapshots from this distribution, cisto-trans nonequilibrium simulations were performed. Given that initially the unbound ligand can be anywhere around the protein, and that the length of the trajectories $(100 \times 1 \,\mu\text{s},$ $10\times10\,\mu s$) is on average too short to ensure the complete binding of the ligand, the overall sampling quality of the photoinduced ligand binding is clearly inferior to the one of the above discussed unbinding process. Nonetheless, the data allow for some general qualitative observations, which are presented in the SI (Fig. S14 and Tab. S9) for completeness. Using 403 contacts, the MoSAIC analysis resulted in eight major clusters, where C3 and C6 are again similar as found before. As may be expected, there are several prominent clusters spanning over the binding pocket, in particular C1, C2 and C4 which connect the ligand to the protein. In line, we find that these clusters as well as C6 exhibit an early response at 1 ns and 60 ns, before all clusters peak at $\sim 3 \,\mu s$. Although the approach of the ligand to the binding pocket facilitates many ligand-protein contacts, the binding process can be still described via a set of contact clusters.

Conclusion

We have shown that the dynamic decomposition of proteins into MoSAIC clusters reveals a dynamics-based modular architecture that enables long-range communication. To assess the validity and generality of this concept, we have adopted four photoswitchable PDZ do-

mains and investigated how different domains, ligands and perturbations affect both the clusters and their dynamical evolution.

MoSAIC analyses across these systems have revealed several recurring contact clusters that represent shared flexible structural modules. Notably, cluster C3 is located at the $\beta_2\beta_3$ -loop, C6 around the $\beta_1\beta_2$ -loop as well as C7 at the α_1 helix. Additional clusters emerge in response to the photoswitch perturbation—specifically, C1 and C2 (at α_3) in PDZ3 domains and C4 (at α_2) in PDZ2 domains. Although the precise contacts comprising a given cluster may vary between systems, exact correspondence is neither expected nor essential. Furthermore, equilibrium MD simulations of PDZ3WT confirm that contact clusters can be identified under equilibrium conditions, reinforcing that such clusters are intrinsic to the protein's architecture.

To investigate how contact clusters mediate protein dynamics and function, we have analyzed the nonequilibrium response of all systems by computing the dynamical content [Eq. (2)], where the peak positions indicate characteristic timescales of the protein's response and can be linked to the motions of individual contact clusters. By comparing two PDZ3 domains with slightly different ligands (Figs. 1 and 3) and two PDZ2 domains—one containing a cross-linked photoswitch (PDZ2S, Fig. 4) and one with a photoswitched ligand (PDZ2L, Fig. 5)—we identified several common features in their dynamical content. Overall, at least three distinct timescales emerge:

- 1 10 ns, corresponding to the local stress initially induced by the photoswitch,
- 100 300 ns, reflecting the response of more distant residues,
- a few μ s, reporting on a global conformational response of the protein.

While a local short-time response to photoswitching is generally expected, it became most evident in the dynamical content of PDZ3, where the initially perturbed cluster C1 contains several contacts in close proximity of the photoswitch. Most interestingly, across all systems, a coupling between the perturbed end of the PDZ domain (e.g., clusters C1 or C4) and

more distal regions (e.g., clusters C6 and C7) occurs on a timescale of about 50 to 200 ns. In PDZ3, this long-range communication has been shown to be mediated by the ligand, which forms multiple contacts linking these clusters. 45 In general, this coupling likely involves several competing mechanical pathways mediated by rigid secondary structures. For the isolated PDZ domains studied here, this long-range interaction does not appear to serve a specific functional purpose. However, if the $\beta_1\beta_2$ -loop or $\beta_3\alpha_1$ -loop of clusters C6 and C7 were to interact with a nearby molecule (such as another protein or cofactor, as discussed in Ref. 22), the formation of new contacts could stabilize the allosteric response of cluster C6. This would lead to an allosteric transition in C6, triggered by C1. For example, the Rho GTPase Cdc42 has been shown to allosterically regulate the Par-6 PDZ domain by binding to β_1 and α_1 .⁵²

The consistent presence of a dominant microsecond-scale response involving nearly all contact clusters is remarkable. While the sub- μ s dynamics discussed above is specific to the system, virtually all contact distances across all systems exhibit this long-time behavior, see Figs. S2, S9, S11 and S13 in the SI. Supporting the view that conformational transitions in proteins are largely governed by diffusive processes, 54-58 the microsecond dynamics of these distances can be well described by a power-law dependence, $r(t) \propto t^{\alpha}$. This is demonstrated for a number of examples in Fig. S17, which reveals that the exponent α typically ranges between 0.3 (anomalous or subdiffusive motion) and 0.5 (normal diffusion). Since our simulation trajectories are limited to $10 \,\mu s$, the observed microsecond-scale response of nearly all distances may indicate that some distances have not yet equilibrated. This observation aligns with experimental findings, ^{28–30} which suggest that the overall photoinduced conformational transition in PDZ domains is not completed before $100 \,\mu s$.

In this Perspective, we have focused on photoswitchable PDZ domains, whose nanosecond—to—microsecond response times enable direct observation of the allosteric transition. Ongoing work extends this analysis to larger al-

losteric systems such as the tetracycline repressor TetR and the heat shock protein Hsp90, for which contact clusters can be readily derived from available microsecond-scale equilibrium simulations. ^{59,60} Identifying which contacts change during a conformational transition also enables the construction of mechanism-informed biasing coordinates for enhanced sampling techniques. ^{61,62} In this way, physics-based, mechanism-guided sampling strategies may effectively complement data-driven machine learning approaches for exploring allosteric mechanisms in proteins.

Methods

MD simulations. All simulations used the GROMACS v2020 software package, ⁶³ the Amber99SB*ILDN force field^{64–66} and the TIP3P water model, ⁶⁷ and were run at a temperature of 300 K, with a coordinate write out time of 20 ps. Table 1 list all systems and simulations, while specific MD details for PDZ3, PDZ2S, and PDZ2L are given in Refs. 31, 15, and 30, respectively. For all systems, first a set of μ slong equilibrium simulations were conducted, from which statistically independent starting configurations for the nonequilibrium runs were obtained. The latter used the potential energy surface switching method by Nguyen et al., ⁶⁸ to mimic the initial photoisomerization of the azobenzene photoswitch. Further details are given for each specific system in the SI.

MoSAIC clustering. In a first step, we determined the inter-residue contacts of each system. Excluding the two nearest neighbors (|i-j|>2 for residues i and j), this is achieved by requesting that the shortest heavy-atom distance between the two residues is below 0.45 nm for at least 10% of the total simulation time. 41,43 To distinguish collective motions underlying functional dynamics and uncorrelated motions, MoSAIC 44 ("Molecular Systems Automated Identification of Cooperativity") analysis calculates the linear or nonlinear 69 correlation matrix between all contact distances. To rearrange this matrix in an approximately block-

diagonal form, we employ a community detection technique called Leiden clustering. To Using the constant Potts model, the user-chosen resolution parameter γ (0 < γ \leq 1) determines the average correlation of the resulting blocks or clusters: larger values of γ yield many highly correlated clusters, while smaller values give few but larger and less correlated clusters. Since MoSAIC is very robust with respect to sparse data, it is sufficient to use only every 5th frame of a trajectory.

Timescale analysis. Each averaged distance is fitted by Eq. (1) using a maximum-entropy method ⁴⁷ that minimizes $\chi^2 - \lambda S_{\text{ent}}$, where χ^2 is the usual root-mean-square deviation and S_{ent} the entropy-based regularization factor. The regularization parameter λ needs to be chosen prior to the analysis and controls over- and under-fitting. For each system, one common value is chosen: $\lambda^{\text{PDZ3}} = 50$, $\lambda^{\text{PDZ3L6}} = 100$, $\lambda^{\text{PDZ2L}} = 200 \text{ and } \lambda^{\text{PDZ2S}} = 50.$ We improve the convergence, precision and stability of the fit by several measures: (1) A linear interpolation between all neighboring frames is employed increasing the number of frames by factor of four. (2) The frames are transformed to be logspaced along the time-axis which ensures that each decade contributes equally with about 750 frames. (3) To suppress fast fluctuations of the data, a low-pass Gaussian filtering ⁵¹ is applied with a standard deviation of $\sigma = 6$ frames. (4) To improve the fit at the upper boundary, the data is extended by one additional order of magnitude by a constant value, derived as average over half of the previous decade.⁷¹

Supplementary material

Includes for all considered proteins their sequence and secondary structure, the MoSAIC correlation matrix, the list of contacts included in the clusters, and their nonequilibrium time evolution.

Acknowledgments

The authors thank Peter Hamm, Steffen Wolf, Georg Diez, Ahmed Ali, Camilla Sordi, and Sofia Sartore for helpful comments and discussions. This work has been supported by the Deutsche Forschungsgemeinschaft (DFG) within the framework of the Research Unit FOR 5099 "Reducing complexity of nonequilibrium" (project No. 431945604), the High Performance and Cloud Computing Group at the Zentrum für Datenverarbeitung of the University of Tübingen and the Rechenzentrum of the University of Freiburg, the state of Baden-Württemberg through bwHPC and the DFG through grant no INST 37/935-1 FUGG (RV bw16I016), and the Black Forest Grid Initiative.

Data Availability Statement

The clustering package MoSAIC is available at our group homepage https://www.moldyn.uni-freiburg.de/software.html. Trajectories and simulation results are available from the authors upon reasonable request.

References

- (1) Wodak, S. J. et al. Allostery in its many disguises: From theory to applications. *Structure* **2019**, *27*, 566–578.
- (2) Gunasekaran, K.; Ma, B.; Nussinov, R. Is allostery an intrinsic property of all dynamic proteins? *Proteins* **2004**, *57*, 433–443.
- (3) Bahar, I.; Chennubhotla, C.; Tobi, D. Intrinsic dynamics of enzymes in the unbound state and relation to allosteric regulation. *Curr. Opin. Struct. Biol.* **2007**, 17, 633–640.
- (4) Cui, Q.; Karplus, M. Allostery and cooperativity revisited. *Protein Science* **2008**, 17, 1295–1307.
- (5) Changeux, J.-P. Allostery and the Monod-Wyman-Changeux Model After 50 Years. *Ann. Rev. Biophys.* **2012**, *41*, 103–133.
- (6) Bowman, G. R.; Geissler, P. L. Equilibrium fluctuations of a single folded protein

- reveal a multitude of potential cryptic allosteric sites. *Proc. Natl. Acad. Sci. USA* **2012**, *109*, 11681–11686.
- (7) Motlagh, H. N.; Wrabl, J. O.; Li, J.; Hilser, V. J. The ensemble nature of allostery. *Nature (London)* **2014**, *508*, 331–339.
- (8) Tsai, C. J.; Nussinov, R. A Unified View of "How Allostery Works". *PLoS Comput. Biol.* **2014**, *10*.
- (9) Thirumalai, D.; Hyeon, C.; Zhuravlev, P. I.; Lorimer, G. H. Symmetry, Rigidity, and Allosteric Signaling: From Monomeric Proteins to Molecular Machines. *Chem. Rev.* 2019, 119, 6788–6821.
- (10) Brüschweiler, S.; Schanda, P.; Kloiber, K.; Brutscher, B.; Kontaxis, G.; Konrat, R.; Tollinger, M. Direct Observation of the Dynamic Process Underlying Allosteric Signal Transmission. J. Am. Chem. Soc. 2009, 131, 3063–3068.
- (11) Mehrabi, P.; Schulz, E. C.; Dsouza, R.; Müller-Werkmeister, H. M.; Tellkamp, F.; Miller, R. J. D.; Pai, E. F. Time-resolved crystallography reveals allosteric communication aligned with molecular breathing. *Science* 2019, 365, 1167–1170.
- (12) Bozovic, O.; Jankovic, B.; Hamm, P. Using azobenzene photocontrol to set proteins in motion. *Nat. Rev. Chem.* **2022**, *6*, 112–124, Publisher: Springer.
- (13) Hyeon, C.; Lorimer, G. H.; Thirumalai, D. Dynamics of allosteric transitions in GroEL. *Proc. Natl. Acad. Sci. USA* **2006**, *103*, 18939 18944.
- (14) Pontiggia, F.; Pachov, D.; Clarkson, M.; Villali, J.; Hagan, M.; Pande, V.; Kern, D. Free energy landscape of activation in a signalling protein at atomic resolution. *Nat. Commun.* **2015**, *6*, 7284.
- (15) Buchenberg, S.; Sittel, F.; Stock, G. Timeresolved observation of protein allosteric

- communication. *Proc. Natl. Acad. Sci. USA* **2017**, *114*, E6804–E6811.
- (16) Zheng, Y.; Cui, Q. Multiple Pathways and Time Scales for Conformational Transitions in apo-Adenylate Kinase. J. Chem. Theory Comput. 2018, 14, 1716–1726.
- (17) Ayaz, P.; Lyczek, A.; Paung, Y.; Mingione, V. R.; Iacob, R. E.; de Waal, P. W.; Engen, J. R.; Seeliger, M.; A. Shan, Y.; Shaw, D. E. Structural mechanism of a drug-binding process involving a large conformational change of the protein target. *Nat. Commun.* **2023**, *14*, 1885.
- (18) Guo, J.; Zhou, H.-X. Protein Allostery and Conformational Dynamics. *Chem. Rev.* **2016**, *116*, 6503–6515.
- (19) Dokholyan, N. V. Controlling Allosteric Networks in Proteins. *Chem. Rev.* **2016**, 116, 6463–6487.
- (20) Fuentes, E.; Der, C.; Lee, A. Ligand-dependent dynamics and intramolecular signaling in a PDZ domain. *J. Mol. Biol.* **2004**, *335*, 1105–1115.
- (21) Petit, C. M.; Zhang, J.; Sapienza, P. J.; Fuentes, E. J.; Lee, A. L. Hidden dynamic allostery in a PDZ domain. *Proc. Natl.* Acad. Sci. USA 2009, 106, 18249–18254.
- (22) Ye, F.; Zhang, M. Structures and target recognition modes of PDZ domains: recurring themes and emerging pictures. *Biochem. J.* **2013**, *455*, 1–14.
- (23) Gautier, C.; Laursen, L.; Jemth, P.; Gianni, S. Seeking allosteric networks in PDZ domains. *Protein Eng. Des. Sel.* **2019**, *31*, 367–373.
- (24) Gerek, Z. N.; Ozkan, S. B. Change in Allosteric Network Affects Binding Affinities of PDZ Domains: Analysis through Perturbation Response Scanning. PLoS Comput. Biol. 2011, 7.
- (25) Kumawat, A.; Chakrabarty, S. Hidden electrostatic basis of dynamic allostery in

- a PDZ domain. *Proc. Natl. Acad. Sci. USA* **2017**, *114*, E5825–E5834.
- (26) Stevens, A. O.; He, Y. Allosterism in the PDZ Family. *Int. J. Mol. Sci.* **2022**, *23*, 1454.
- (27) Faure, A. J.; Domingo, J.; Schmiedel, J. M.; Hidalgo-Carcedo, C.; Diss, G.; Lehner, B. Mapping the energetic and allosteric landscapes of protein binding domains. *Nature* **2022**, 604, 175–183.
- (28) Bozovic, O.; Ruf, J.; Zanobini, C.; Jankovic, B.; Buhrke, D.; Johnson, P. J. M.; Hamm, P. The Speed of Allosteric Signaling Within a Single-Domain Protein. J. Phys. Chem. Lett. 2021, 12, 4262– 4267.
- (29) Buchli, B.; Waldauer, S. A.; Walser, R.; Donten, M. L.; Pfister, R.; Bloechliger, N.; Steiner, S.; Caflisch, A.; Zerbe, O.; Hamm, P. Kinetic response of a photoperturbed allosteric protein. *Proc. Natl. Acad. Sci. USA* 2013, 110, 11725–11730.
- (30) Bozovic, O.; Zanobini, C.; Gulzar, A.; Jankovic, B.; Buhrke, D.; Post, M.; Wolf, S.; Stock, G.; Hamm, P. Real-time observation of ligand-induced allosteric transitions in a PDZ domain. *Proc. Natl. Acad. Sci. USA* **2020**, *117*, 26031 26039.
- (31) Ali, A. A. A. I.; Gulzar, A.; Wolf, S.; Stock, G. Nonequilibrium Modeling of the Elementary Step in PDZ3 Allosteric Communication. *J. Phys. Chem. Lett.* **2022**, 13, 9862–9868.
- (32) Noé, F.; Clementi, C. Collective variables for the study of long-time kinetics from molecular trajectories: theory and methods. *Curr. Opin. Struct. Biol.* **2017**, *43*, 141 147.
- (33) Sittel, F.; Stock, G. Perspective: Identification of Collective Coordinates and Metastable States of Protein Dynamics. *J. Chem. Phys.* **2018**, *149*, 150901.

- (34) Sittel, F.; Filk, T.; Stock, G. Principal component analysis on a torus: Theory and application to protein dynamics. *J. Chem. Phys.* **2017**, *147*, 244101.
- (35) Bowman, G. R., Pande, V. S., Noé, F., Eds. An introduction to Markov state models and their application to long timescale molecular simulation; Advances in experimental medicine and biology 797; Springer, 2014.
- (36) Wang, W.; Cao, S.; Zhu, L.; Huang, X. Constructing Markov State Models to elucidate the functional conformational changes of complex biomolecules. *WIREs Comp. Mol. Sci.* **2018**, *8*, e1343.
- (37) Scherer, M. K.; Husic, B. E.; Hoffmann, M.; Paul, F.; Wu, H.; Noé, F. Variational selection of features for molecular kinetics. *J. Chem. Phys.* **2019**, *150*, 194108.
- (38) Nagel, D.; Sartore, S.; Stock, G. Selecting Features for Markov Modeling: A Case Study on HP35. *J. Chem. Theory Comput.* **2023**, *19*, 3391 3405.
- (39) Latzer, J.; Shen, T.; Wolynes, P. G. Conformational Switching upon Phosphorylation: A Predictive Framework Based on Energy Landscape Principles. *Biochem.* **2008**, *47*, 2110–2122.
- (40) Di Paola, L.; De Ruvo, M.; Paci, P.; Santoni, D.; Giuliani, A. Protein Contact Networks: An Emerging Paradigm in Chemistry. Chem. Rev. 2013, 113, 1598–1613.
- (41) Ernst, M.; Sittel, F.; Stock, G. Contactand distance-based principal component analysis of protein dynamics. *J. Chem. Phys.* **2015**, *143*, 244114.
- (42) Ernst, M.; Wolf, S.; Stock, G. Identification and validation of reaction coordinates describing protein functional motion: Hierarchical dynamics of T4 Lysozyme. *J. Chem. Theory Comput.* **2017**, *13*, 5076 5088.

- (43) Yao, X.-Q.; Momin, M.; Hamelberg, D. Establishing a Framework of Using Residue—Residue Interactions in Protein Difference Network Analysis. *J. Chem. Inf. Model.* **2019**, *59*, 3222–3228.
- (44) Diez, G.; Nagel, D.; Stock, G. Correlation-based feature selection to identify functional dynamics in proteins. *J. Chem. Theory Comput.* **2022**, *18*, 5079 5088.
- (45) Ali, A. A. A. I.; Dorbath, E.; Stock, G. Allosteric communication mediated by protein contact clusters: A dynamical model. J. Chem. Theory Comput. 2024, 20, 10731 – 10739.
- (46) Stock, G.; Hamm, P. A Nonequilibrium Approach to Allosteric Communication. *Phil. Trans. B* **2018**, *373*, 20170187.
- (47) Lórenz-Fonfría, V. A.; Kandori, H. Transformation of Time-Resolved Spectra to Lifetime-Resolved Spectra by Maximum Entropy Inversion of the Laplace Transform. *Appl. Spectrosc.* **2006**, *60*, 407–417.
- (48) Papaleo, E.; Saladino, G.; Lambrughi, M.; Lindorff-Larsen, K.; Gervasio, F. L.; Nussinov, R. The Role of Protein Loops and Linkers in Conformational Dynamics and Allostery. *Chem. Rev.* 2016, 116, 6391–6423.
- (49) Nagel, D.; Stock, G. msmhelper: A Python package for Markov state modeling of protein dynamics. J. Open Source Softw. 2023, 8, 5339.
- (50) Zhou, T.; Caflisch, A. Distribution of Reciprocal of Interatomic Distances: A Fast Structural Metric. J. Chem. Theory Comput. 2012, 8, 2930 2937.
- (51) Nagel, D.; Sartore, S.; Stock, G. Toward a Benchmark for Markov State Models: The Folding of HP35. *J. Phys. Chem. Lett.* **2023**, *14*, 6956–6967.
- (52) Peterson, F. C.; Penkert, R. R.; Volkman, B. F.; Prehoda, K. E. Cdc42 Regulates the Par-6 PDZ Domain through

- an Allosteric CRIB-PDZ Transition. *Mol. Cell* **2004**, *13*, 665–676.
- (53) Li, H.; Ma, A. Enhanced sampling of protein conformational changes via true reaction coordinates from energy relaxation. *Nat Commun* **2025**, *16*, 786.
- (54) Zwanzig, R. Diffusion in rough potentials. *Proc. Natl. Acad. Sci.* (USA) **1988**, 85, 2029.
- (55) Neusius, T.; Daidone, I.; Sokolov, I. M.; Smith, J. C. Subdiffusion in Peptides Originates from the Fractal-Like Structure of Configuration Space. *Phys. Rev. Lett.* **2008**, *100*, 188103.
- (56) Best, R. B.; Hummer, G. Coordinatedependent diffusion in protein folding. *Proc. Natl. Acad. Sci. USA* **2010**, *107*, 1088 – 1093.
- (57) Volkhardt, A.; Grubmüller, H. Estimating ruggedness of free-energy landscapes of small globular proteins from principal component analysis of molecular dynamics trajectories. *Phys. Rev. E* **2022**, *105*, 044404.
- (58) Janke, P.; Dorbath, E.; Stock, G.; Hamm, P. Perspective: Universal Relaxation Behaviour of Photoactive Proteins. J. Chem. Phy. 2025,
- (59) Yuan, Y.; Deng, J.; Cui, Q. Molecular Dynamics Simulations Establish the Molecular Basis for the Broad Allostery Hotspot Distributions in the Tetracycline Repressor. J. Am. Chem. Soc. 2022, 144, 10870–10887.
- (60) Wolf, S.; Sohmen, B.; Hellenkamp, B.; Thurn, J.; Stock, G.; Hugel, T. Hierarchical dynamics in allostery following ATP hydrolysis monitored by single molecule FRET measurements and MD simulations. *Chem. Sci.* **2021**, *12*, 3350–3359.
- (61) Chipot, C.; Pohorille, A. Free Energy Calculations; Springer: Berlin, 2007.

- (62) Mehdi, S.; Smith, Z.; Herron, L.; Zou, Z.; Tiwary, P. Enhanced Sampling with Machine Learning. *Annu. Rev. Phys. Chem.* **2024**, *75*, 347–370.
- (63) Abraham, M. J.; Murtola, T.; Schulz, R.; Pall, S.; Smith, J. C.; Hess, B.; Lindahl, E. GROMACS: High performance molecular simulations through multi-level parallelism from laptops to supercomputers. *SoftwareX* **2015**, *1-2*, 19 25.
- (64) Hornak, V.; Abel, R.; Okur, A.; Strockbine, B.; Roitberg, A.; Simmerling, C. Comparison of multiple Amber force fields and development of improved protein backbone parameters. *Proteins* **2006**, *65*, 712–725.
- (65) Best, R. B.; Hummer, G. Optimized Molecular Dynamics Force Fields Applied to the Helix-Coil Transition of Polypeptides. J. Phys. Chem. B 2009, 113, 9004– 9015.
- (66) Lindorff-Larsen, K.; Piana, S.; Palmo, K.; Maragakis, P.; Klepeis, J. L.; Dror, R. O.; Shaw, D. E. Improved side-chain torsion potentials for the Amber ff99SB protein force field. *Proteins* 2010, 78, 1950–1958.
- (67) Jorgensen, W. L.; Chandrasekhar, J.; Madura, J. D.; Impey, R. W.; Klein, M. L. Comparison of simple potential functions for simulating liquid water. J. Chem. Phys. 1983, 79, 926–935.
- (68) Nguyen, P. H.; Gorbunov, R. D.; Stock, G. Photoinduced Conformational Dynamics of a Photoswitchable Peptide: A Nonequilibrium Molecular Dynamics Simulation Study. *Biophys. J.* 2006, 91, 1224–1234.
- (69) Nagel, D.; Diez, G.; Stock, G. Accurate estimation of the normalized mutual information of multidimensional data. *J. Chem. Phys.* **2024**, *161*, 054108.
- (70) Traag, L., V. A. and Waltman; van Eck, N. J. From Louvain to Leiden: guaranteeing well-connected communities. *Sci. Rep.* **2019**, *9*, 5233.

(71) Dorbath, E.; Gulzar, A.; Stock, G. Logperiodic oscillations as real-time signatures of hierarchical dynamics in proteins. *J. Chem. Phys.* **2024**, *160*, 074103.

TOC Graphic

